AD-A278 866

(4)

CONTRACT TECHNICAL REPORT

"A Mechanics Mode for the Compressive Response of Fiber Reinforced Composites"

By

I. Chung and Y. Jack Weitsman

Prepared for: Office of Naval Research
Arlington, Virginia

Mechanics Division
Engineering Science Directorate
Contract N00014-90-J-1556

Report ESM93-2.0-CM
May 1993

Engineering Science and Mechanics
THE UNIVERSITY OF TENNESSEE
Knoxville, TN 37996-2030

Unclassified

SECURITY CLASSIFICATION OF THIS PAGE

REPORT DOCUMENTATION PAGE

1a. REPORT SECURITY CLASSIFICATION Unclassified	1b. RESTRICTIVE MARKINGS
2a. SECURITY CLASSIFICATION AUTHORITY	3. DISTRIBUTION/AVAILABILITY OF REPORT Unlimited
2b. DECLASSIFICATION/DOWNGRADING SCHEDULE	
4. PERFORMING ORGANIZATION REPORT NUMBER(S)	5. MONITORING ORGANIZATION REPORT NUMBER(S)
6a. NAME OF PERFORMING ORGANIZATION Eng. Science & Mechanics University of Tennessee 6b. OFFICE SYMBOL (If applicable)	7a. NAME OF MONITORING ORGANIZATION Office of Naval Research
6c. ADDRESS (City, State, and ZIP Code) 307 Perkins Hall Knoxville, TN 37996-2030	7b. ADDRESS (City, State, and ZIP Code) Office of Naval Research, Code 432 800 N. Quincy Ave., Ballston Tower #1 Arlington, VA 22217
8a. NAME OF FUNDING/SPONSORING ORGANIZATION Office of Naval Research 8b. OFFICE SYMBOL (If applicable)	9. PROCUREMENT INSTRUMENT IDENTIFICATION NUMBER N00014-90-J-1556 (ONR Contract #)
8c. ADDRESS (City, State, and ZIP Code) Arlington, VA 22217	10. SOURCE OF FUNDING NUMBERS PROGRAM ELEMENT NO. / PROJECT NO. / TASK NO. / WORK UNIT ACCESSION NO

11. TITLE (Include Security Classification) A Mechanics Model for the Compressive Response of Fiber Reinforced Composites

12. PERSONAL AUTHOR(S) I. Chung and Y. Jack Weitsman

13a. TYPE OF REPORT	13b. TIME COVERED	14. DATE OF REPORT (Year, Month, Day)	15. PAGE COUNT
Technical	FROM 1/1/93 TO 12/31/94	94/03/29	30

16. SUPPLEMENTARY NOTATION

17. COSATI CODES			18. SUBJECT TERMS (Continue on reverse if necessary and identify by block number)
FIELD	GROUP	SUB-GROUP	

19. ABSTRACT (Continue on reverse if necessary and identify by block number)

This article presents a model for the uni-axial compressive response of uni-directionally reinforced fibrous composite. The model accounts for the non-linear shear response and the failure strain of the matrix, incorporating both aspects into a non-linear field equation which governs the load-deflection process. In addition, the model considers the effects of two kinds of geometric imperfections, namely, initial fiber waviness and random fiber spacing. It is shown that under uni-axial compression random fiber spacing may instigate the formation of severe transverse loadings on the fibers, which suggest the existence of a transitional mechanism from micro-buckling to micro-kinking.

Computational results are presented which illuminate the effects of several material and geometric factors on the compressive strength of composites.

20. DISTRIBUTION/AVAILABILITY OF ABSTRACT ☐ UNCLASSIFIED/UNLIMITED ☐ SAME AS RPT. ☐ DTIC USERS	21. ABSTRACT SECURITY CLASSIFICATION Unclassifed
22a. NAME OF RESPONSIBLE INDIVIDUAL Dr. Yapa Rajapakse	22b. TELEPHONE (Include Area Code) 703/696-4403 / 22c. OFFICE SYMBOL

DD FORM 1473, 84 MAR

83 APR edition may be used until exhausted.
All other editions are obsolete.

SECURITY CLASSIFICATION OF THIS PAGE

Unclassified

A MECHANICS MODEL FOR THE COMPRESSIVE RESPONSE OF FIBER REINFORCED COMPOSITES

I. Chung § and Y. Weitsman § ◊

ABSTRACT

This article presents a model for the uni-axial compressive response of uni-directionally reinforced fibrous composite. The model accounts for the non-linear shear response and the failure strain of the matrix, incorporating both aspects into a non-linear field equation which governs the load-deflection process. In addition, the model considers the effects of two kinds of geometric imperfections, namely, initial fiber waviness and random fiber spacing. It is shown that under uni-axial compression random fiber spacing may instigate the formation of severe transverse loadings on the fibers, which suggest the existence of a transitional mechanism from micro-buckling to micro-kinking.

Computational results are presented which illuminate the effects of several material and geometric factors on the compressive strength of composites.

§Department of Engineering Science and Mechanics,The University of Tennessee at Knoxville
◊Engineering Technology Division, Oak Ridge National Laboratory

1. INTRODUCTION

The compressive behavior of composite materials has been studied extensively during the past three decades and a review of literature on the subject is beyond the scope of this paper. Substantial listings of references on the subject can be found in the articles by Shuart (1985), Camponeschi (1991), Guynn et al. (1992) and Piggott (1993). Suffices to say that the compressive response of composites was found to depend on the properties and response of the constituent materials and on the fiber volume fraction. As may be expected, compressive strength is sensitive to imperfections.

The essential novel feature in the present work is the incorporation of random fiber spacings, as commonly encountered in composites, into a model for their compressive behavior. The main consequence of the foregoing feature is that it predicts a response which involves the emergence of highly concentrated lateral forces on the fibers simultaneously with micro-buckling. These lateral forces are a most likely cause for the development of kinks. One of the outstanding issues regarding the compressive response of composites is that the common methodology for predicting compressive failure stems from considerations of buckling and stability, while most failed specimens exhibit localized kink bands which span the thicknesses of the test coupons. It seems that all other models address micro-buckling and micro-kinking exclusively of each other, and can thus be grouped accordingly:

(1) Models which consider buckling. These include the work of Rosen (1965), which seems to be the first article on compressive failure of composites. Considering "shear -mode buckling" that model predicted a failure stress $\sigma_{CR} = G_m / (1 - V_f)$, where G_m is the shear modulus of the matrix and V_f the fiber volume fraction. That prediction is inadequate for two reasons: (a) it gives σ_{CR} which is several times higher than experimental values, (b) the relation $\sigma_{CR} \sim 1 / (1 - V_f)$ contradicts experimental observations which show that σ_{CR} grows linearly with V_f (at least up to $V_f \approx 0.55$) (e.g. Piggott and Harris (1980), Morley (1987)).

Several modifications to Rosen's model were introduced subsequently. Primarily, these modifications considered non-linear shear response of the matrix and initial fiber waviness (e.g. Wang (1978), Lin and Zhang (1992), Guynn et al. (1992), Highsmith et al. (1992) and others listed in the aforementioned review articles). Additional modifications included the incorporation of fibers' shear-deformation, such as by Davis (1975), or the accounting for large deformations of the fibers by Yin (1992). Though the latter model stems from a buckling formulation, it is worth noting that it proposes a criterior for kink formation, which occurs when fibers' curvature attains a critical value.

(2) Models which consider the a-priori existence of kinks: These include works by Evans and Adler (1978), Hahn and Williams (1986), and Budiansky and Fleck (1992).

The compressive response of multi-directionally reinforced laminates such as Shuart (1989) and of cylindrical shells such as Blake and Starbuck (1993) is beyond the scope of this article. Suffices to say that these complex circumstances activate various modes of failure which do not occur in the uni-directional case considered herein.

In all the above works the fiber reinforced composites were viewed as lamellar regions which consist of fiber and matrix layers as shown in Figure 1a. It should be noted that several investigators (Sadowsky et al. (1967), Herrmann et al. (1967), Lanir and Fung (1972) and Greszczuk (1975)) considered fibers of cylindrical geometry. All those works assumed linear elastic behavior of fiber and matrix materials.

In addition to random fiber spacing the current model includes initial fiber waviness and considers the non-linear shear stress-strain response in the matrix. The fibers are assumed to deform in accordance with classical beam theory.

2. FORMULATION AND RESULTS

Consider a uni-axially reinforced composite which, following Rosen (1965), is represented by a two-dimensional layered array as shown in Figure 1(a). Let x and y denote Cartesian coordinates in directions parallel and transverse to the layers, and designate by 2h the thickness of a "fiber layer" centered within a composite layer of thickness 2c. Consequently we have $V_f = h/c$ and $V_m = (c-h)/c$, where V_f and V_m are fiber and matrix volume fractions, respectively.

We focus attention on the "shear mode" of buckling (Rosen (1965), Garg et al. (1973)), where all fibers buckle in phase. Then, following Rosen's premises (1965) for high performance composite material systems, we assume that the external compressive load N is borne entirely by the fiber region, which is modelled as a Bernoulli-Euler beam, while the matrix responds in shear only. Consequently, we have the following familiar expression for γ^m_{xy}, the shear strain in the matrix:

$$\gamma^m_{xy} = \frac{1}{1-V_f}\frac{dv^f}{dx} \tag{1}$$

In equation (1) v^f denotes the lateral displacement (in the y-direction) of the fiber. In view of the assumption of Bernoulli-Euler theory, v^f, and thereby also γ^m_{xy}, depends only on x.

In addition, we consider a micro-buckling length L and and initial fiber waviness $v^f_0(x)$ with periodicity of 2L. In the sequel, we let $v^f_0(x) = \delta_0 \cos(\pi x/L)$, though this

specific choice is not essential to our method. Finally, in anticipation of the circumstances which emerge due to non-uniform fiber spacings, we denote by q(x) the distributed lateral load on the fiber. See Figure 1(b).

Considering non-linear shear response of the matrix, we write

$$\tau^m_{xy} = G^m_e \, F\,(\gamma^m_{xy}) \tag{2}$$

where the function $F(\gamma^m_{xy})$ expresses that non-linear shear behavior of the matrix scaled by the initial shear modulus G^m_e.

The longitudinal strain in the fiber, ε^f_x, under the combined effects of compression and bending is given by

$$\varepsilon^f_x = \frac{du^f}{dx} + \frac{1}{2}\left[\left(\frac{dv^f}{dx} + \frac{dv^f_0}{dx}\right)^2 - \left(\frac{dv^f_0}{dx}\right)^2\right] - y\,\frac{d^2v^f}{dx^2} \tag{3}$$

In equation (3), u^f denotes the fiber displacement in the direction of x.

Consequently, the axial displacement at x = L/2 is given by

$$u^f_{x=L/2} = \Delta = \frac{1}{2}\int_0^{L/2} \left[\left(\frac{dv^f}{dx} + \frac{dv^f_0}{dx}\right)^2 - \left(\frac{dv^f_0}{dx}\right)^2\right] dx + \frac{1}{2}\,\frac{NL}{EA} \tag{4}$$

As can be noted from equations (3) and (4) the hypothesis that fibers deform in-phase implies that u^f and v^f are common to all fibers regardless of their spacing. On the other hand, equations (1) and (2) state that the support provided by the matrix varies with the fiber volume fraction V_f. These observations imply the existence of lateral loads, q = q(x), which enforce a common, in-phase deformation of all fibers in the case of non-uniform spacing. To emphasize their dependence of the spacing c, we shall write q = q(x,c).

Consider an individual cell of width 2c. The principle of virtual work yields

$$\int_{V^f} \sigma^f_x \,\delta\varepsilon^f_x \, dV^f + \int_{V^m} \tau^m_{xy}\,\delta\gamma^m_{xy}\, dV^m - \int_0^{L/2} q(x,c)\,\delta v^f dx + N\,\delta\Delta = 0 \tag{5}$$

Substitution of expressions (1)-(4) into equation (5) and employment of integrations by parts yield the following field equation and boundary conditions for each individual cell:

$$EI_f \frac{d^4v^f}{dx^4} - 2cG_e^m \frac{d}{dx} F\left(\frac{1}{1-V_f}\frac{dv^f}{dx}\right) + N\left(\frac{d^2v^f}{dx^2} + \frac{d^2v_0^f}{dx^2}\right) = q(x,c) \tag{6}$$

with

$$\begin{aligned} &\frac{dv^f}{dx} = 0, \quad \frac{d^3v^f}{dx^3} = 0 \quad \text{at} \quad x = 0 \\ &v^f = 0, \quad \frac{d^2v^f}{dx^2} = 0 \quad \text{at} \quad x = \frac{L}{2} \end{aligned} \tag{7}$$

Note that in view of the non-linearity of F in its argument equation (6) is a non-linear differential equation for v^f.

Turning to the case of random fiber spacing, let p(c) denote the probability density of the cell dimension 2c. Obviously

$$\int_h^\infty p(c)\, dc = 1 \tag{8}$$

In the present circumstance the principle of virtual work gives

$$\int_h^\infty p(c) \left\{ \int_{V^f} \sigma_x^f\, \delta\varepsilon_x^f\, dV^f + \int_{V^m} \tau_{xy}^m\, \delta\gamma_{xy}^m\, dV^m - \int_0^{L/2} q(x,c)\, \delta v^f\, dx + N\, \delta\Delta \right\} dc = 0 \tag{9}$$

Furthermore, in the absence of external lateral loads, equilibrium in the direction of y requires

$$\int_h^\infty p(c) \left(\int_0^{L/2} q(x,c)\, dx \right) dc = 0 \tag{10}$$

Integration-by-parts of equation (9), upon expressing all variations in terms of $\delta(\frac{dv^f}{dx})$, gives the following field equation for v^f

$$EI_f \frac{d^3v^f}{dx^3} - \int_h^\infty 2c\, p(c)\; G_e^m \frac{d}{dx} F\left(\frac{1}{1-V_f}\frac{dv^f}{dx}\right) dc + N\left(\frac{dv^f}{dx} + \frac{dv_0^f}{dx}\right) = 0 \tag{11}$$

The boundary conditions for the case of randomly spaced fiber remain the same as those given in equations (7).*

It is advantageous to further reduce the order of the differential equation given in (11) and express it in a non-dimensional form in terms of the following non-dimensional parameters:

$$X = \frac{x}{L}, \quad Y = \frac{dv^f}{dx}, \quad \varepsilon = \frac{\delta_0}{L} \tag{12}$$

In addition, the probability distribution function p(c) can be converted to a probability distribution function $\widehat{p}\,(V_f)$.

In view of expressions (12), the non-dimensional form of Equation (11) reads

$$\frac{d^2Y}{dX^2} - \int_0^1 \widehat{p}(V_f)\, \alpha^2\, (1\text{-}V_f)\, F\left(\frac{Y}{1\text{-}V_f}\right) dV_f + \lambda^2 Y = -\lambda^2 Y_o \tag{13}$$

where

$$\alpha^2 = \frac{2h}{V_f\,(1-V_f)}\,\frac{G_e^m L^2}{EI_f}\ , \quad \lambda^2 = \frac{NL^2}{EI_f}\ , \quad Y_o = -\,\varepsilon\pi\, \sin \pi X \tag{14}$$

The boundary conditions which accompany the second order non-linear differential equation (13) are

$$Y(0) = 0, \qquad \frac{dY}{dX}\left(\frac{1}{2}\right) = 0 \tag{15}$$

In the case of uniform fiber spacing equation (13) reduces to

$$\frac{d^2Y}{dX^2} - \alpha^2(1\text{-}V_f)\, F\left(\frac{Y}{1\text{-}V_f}\right) + \lambda^2 Y = -\lambda^2 Y_o \tag{16}$$

Note that for the linearly elastic case with uniformly spaced fibers $F(Y/(1 - V_f)) = Y/(1-V_f)$ and equation (16) takes the simple form

$$\frac{d^2Y}{dX^2} - \alpha^2\, Y + \lambda^2 Y = -\lambda^2 Y_o$$

---

* In view of equation (10) it was possible to derive differential equation (11) which is one order lower than that given in equation (6). The lower order equation (11) enables the determination of the lateral displacement v^f to within a rigid translation, which is of no relevance to the failure mechanisms considered in this work. An additional integration of expression (11) with respect to x, further reduces the order of the differential equation, leading to a solution which incorporates an indeterminate rigid body rotation.

with the solution

$$Y = \frac{\varepsilon\pi\lambda^2}{\lambda^2 - \pi^2 - \alpha^2} \sin \pi X$$

This corresponds to the buckling load predicted by Rosen (1965), namely $\lambda^2 = \pi^2 + \alpha^2$. Note that the above result assumed that the magnitude of the linearly elastic shear strain in the matrix is not limited by any ultimate or plastic level.

However, if one considers a linearly elastic matrix response followed by an ideally plastic deformation at $\gamma^m_{xy} = \gamma_p$, then plastic yield begins at $X = 1/2$ and the onset of plastic deformation is found to occur at

$$\lambda^2 = \frac{(\pi^2 + \alpha^2)\,(1\text{-}V_f)\gamma_p}{\varepsilon\pi + \,(1\text{-}V_f)\gamma_p} = \lambda^2(\gamma_p) \tag{17}$$

The above result agrees with the value obtained by Steif (1988) for the slippage initiation load, beyond which the matrix no longer supports the deformed fibers.

Case 1: Uniformly Spaced Fibers with Bi-linear Shear Modulus of the Matrix

Consider a bilinear shear stress-strain response of the matrix material, given by the following expression for $F(\gamma^m_{xy})$

$$G^m_e F(\gamma_{xy}) = \begin{cases} G^m_p\,(\gamma_{xy} - \gamma_y) + G^m_e\,\gamma_y & \text{if} \quad \gamma_{xy} > \gamma_y \\ G^m_e \gamma_{xy} & \text{if} \quad -\gamma_y < \gamma_{xy} < \gamma_y \\ G^m_p(\gamma_{xy} + \gamma_y) - G^m_e\,\gamma_y & \text{if} \quad \gamma_{xy} < -\gamma_y \end{cases} \tag{18}$$

In equation (18) γ_y is the strain level where the slope of the bi-linear stress-strain diagram changes from an initial value G^m_e to the strain-hardening value G^m_p. It will be shown in this section that the buckling associated with the response expressed in equations (18) can be handled analytically.

For loads that correspond to λ^2 which exceeds $\lambda^2(\gamma_y)$ in equation (17) the shear response of the matrix will follow the bi-linear stress-strain relation over a region $\xi<X<1/2$, but will still remain linearly elastic within the central region $0<X<\xi$. Obviously ξ decreases with increasing λ^2. Substitution of expressions (18) into equation (16) gives

$$\frac{d^2Y}{dX^2} - \alpha_e^2 Y + \lambda^2 Y = -\lambda^2 Y_o \qquad \text{at} \qquad 0 < X < \xi$$
$$\frac{d^2Y}{dX^2} - \alpha_p^2 Y + \lambda^2 Y = -\lambda^2 Y_o - \beta^2 \quad \text{at} \qquad \xi < X < \frac{1}{2} \tag{19}$$

where α_e and α_p defined according to (14) with shear moduli G_e^m and G_p^m, respectively, and

$$\beta^2 = \frac{2h}{V_f(1-V_f)} \frac{(G_e^m - G_p^m)L^2}{EI_f} \gamma_y$$

The boundary and continuity conditions associated with equations (19) are

$$\frac{dY}{dX}(\frac{1}{2}) = 0,\ Y(0) = 0,\ Y(\xi^+) = Y(\xi^-),\ \frac{dY}{dX}(\xi^+) = \frac{dY}{dX}(\xi^-),\ Y(\xi) = -V_m\gamma_y \tag{20}$$

The above conditions correspond, respectively, to the vanishing of the moment at x=L/2, and of the shear at x=0, the continuity of shear and moment at x=ξL and the requirement that, by hypothesis, $|\gamma_{xy}^m| = \gamma_y$ at x=ξL. The five conditions given in equations (20) determine the four unknowns associated with the two second order differential equations (19), as well as the yet unknown location ξ.

Note that the solution for Y determines the displacement v^f to within arbitrary rigid translations and rotations, which are determined from the requirement of continuity of v^f and $\frac{dv^f}{dx}$ at x=ξL, as well as $v^f(0) = 0$ and $\frac{dv^f}{dx} = 0$ at x=L/2.

The solution to equations (19) reads:

for 0<X<ξ

$$Y_-(X) = -\frac{\sinh \kappa_e X}{\sinh \kappa_e \xi}\left\{\frac{\varepsilon\pi\lambda^2}{\lambda^2 - \pi^2 - \alpha_e^2} \sin \pi\xi + (1-V_f)\gamma_y\right\} + \frac{\varepsilon\pi\lambda^2}{\lambda^2 - \pi^2 - \alpha_e^2} \sin \pi X \tag{21}$$

for ξ<X<1/2 and $\lambda^2 < \alpha_p^2$

$$Y_+(X) = -\frac{\cos \kappa_p(1-2X)/2}{\cos \kappa_p(1-2\xi)/2}\left\{\frac{\varepsilon\pi\lambda^2}{\lambda^2 - \pi^2 - \alpha_p^2} \sin \pi\xi + (1-V_f)\gamma_y - \frac{\beta^2}{\lambda^2 - \alpha_p^2}\right\} \tag{22a}$$

$$+\frac{\varepsilon\pi\lambda^2}{\lambda^2-\pi^2-\alpha_\beta^2}\sin\pi X-\frac{\beta^2}{\lambda^2-\alpha_\beta^2}$$

while for $\xi<X<1/2$ and $\lambda^2>\alpha_p^2$

$$Y_+(X)=-\frac{\cosh\kappa_p(1-2X)/2}{\cosh\kappa_p(1-2\xi)/2}\left\{\frac{\varepsilon\pi\lambda^2}{\lambda^2-\pi^2-\alpha_\beta^2}\sin\pi\xi+(1-V_f)\gamma_y-\frac{\beta^2}{\lambda^2-\alpha_\beta^2}\right\} \quad (22b)$$

$$+\frac{\varepsilon\pi\lambda^2}{\lambda^2-\pi^2-\alpha_\beta^2}\sin\pi X-\frac{\beta^2}{\lambda^2-\alpha_\beta^2}$$

In the above equations $\kappa_e=\sqrt{\alpha_\xi^2-\lambda^2}$ and $\kappa_p=\sqrt{|\alpha_\beta^2-\lambda^2|}$.

Equations (21) and (22) match all the conditions (20) except the continuity $\frac{dY}{dX}(\xi^+)=\frac{dY}{dX}(\xi^-)$. The latter condition yields a characteristic equation, upon differentiation of equations (21) and (22), which relates the position of ξ to the load parameter λ^2. This characteristic equation must be solved numerically, with the physically meaningful solution corresponding to the lowest value of λ^2.

In our computations we utilized the constituent properties reported by Guynn et al. (1992) for AS4/PEEK at 21° C. Accordingly, we took $E_f = 67$ GPa, $L = 330$ μm and $\delta_o = 1.65$ μm and $V_f = 0.6$. For purposes of comparison we also considered additional values of V_f in the sequel. The non-linear shear stress-strain response was approximated by a bi-linear relationship with $G_e^m = 1.3$ GPa, $G_p^m = 0.33$ GPa and $\gamma_y = 4.2\%$.

The resulting stress-deflection curves are shown in Figure 2 for various values of V_f. The symbols "+" on those curves correspond to load and displacement values at onset of departure from linearity in the shear stress-strain response of the matrix. Such departure occurs when $|\gamma_{XY}^m| = \gamma_y$ at X = 1/2. Note that when $V_f = 0.9$ the composite can carry compressive loads which exceed the level which cause departure from linear matrix response. However, for $V_f = 0.3$ and $V_f = 0.6$ the stress-deflection curves exhibit the so called "finite disturbance buckling behavior," resembling the buckling of cylindrical shells under uniaxial compression or spherical shells under external pressure (Simitses (1976)). It is interesting to note that for $V_f = 0.3$ and $V_f = 0.6$ the cusps in the stress-deflection curves, which correspond to maximal load levels prior to buckling, occur at magnitudes just above those which cause $|\gamma_{XY}^m| = \gamma_y$ at X=1/2. It is obvious that the theoretically predicted cusps for $V_f =$

0.3 and 0.6 cannot be realized experimentally. Under load controlled tests the maximal loads will be followed by total collapse and under displacement controlled circumstances the specimen would snap through to the lower load levels along the vertical dashed lines shown in Figure 2.

Further insight into the compressive response predicted by the solution to equations (19) and (20) is provided in Figures 3 and 4. The dimensionless length $\hat{\xi}$ ($\hat{\xi}$=1/2 - ξ) of the regions where the matrix shear strain $|\gamma^m_{xy}|$ exceeds the linear elastic limit γ_y is plotted vs. the applied compressive stress σ_c in Figure 3 for fiber volume fractions V_f = 0.3, 0.6 and 0.9. Note that σ_c increases monotonically with $\hat{\xi}$ for V_f = 0.9, but decreases (after very slight initial amplifications) for V_f = 0.3 and 0.6.

The variation of the matrix shear strain γ^m_{xy} with the dimensionless distance X along the fiber/matrix interfaces is shown in Figure 4 for V_f = 0.6. The four curves in that figure correspond to distinct levels of non-dimensional load λ. The top curve, with λ = 23.10 represents typical linear elastic results, with $|\gamma^m_{xy}| < \gamma_y$ for all X and thereby also $\hat{\xi}$ = 0. In this case we obtain a sinusoidal variation of γ^m_{xy} which agrees with earlier results (Wang (1978), Lin and Zhang (1992)), namely $\gamma^m_{xy} = A \sin\pi X$ with $A = \varepsilon\pi\lambda^2 / [(1-V_f)(\lambda^2-\pi^2-\alpha^2)]$. The foregoing sinusoidal variation persists until the onset of inelastic response at X=1/2 which occurs at $\lambda = \lambda_y$ = 30.79. This result is shown by the dashed line in Figure 4. The maximal value of the compressive load, associated with $\lambda = \lambda_{max}$ = 30.81, corresponds to an inelastic zone of dimensionless length $\hat{\xi}$ = 0.05. In this case the variation of γ^m_{xy} with X, shown by the dotted line in Figure 4, is no longer sinusoidal. Beyond $\hat{\xi}$ = 0.05 values of λ decrease while Δ/L increase according to Figure 2. A typical circumstance, corresponding to $\hat{\xi}$ = 0.1 and λ = 30.23, is shown by the solid line in Figure 4.

Case 2: Non-Uniformly Spaced Fibers

Statistical Considerations of Cell-Size Distributions

As noted in the Introduction, non-uniformity in fiber spacing introduces a new aspect into the compressive and buckling behavior of fiber reinforced composites, namely transverse internal lateral loads associated with the common deformation of the fibers. Following the statistics of spatially distributed data and the concept of Voronoi cell tessellation, as employed to represent the spatial distribution of spherical and cylindrical inclusions (Davy and Guild (1988)), we assume a cumulative distribution function for the cell size 2c described by a Poisson's point process

$$P(C > c) = \exp(-2\mu c) \tag{23}$$

In equation (23) μ is the frequency of Voronoi cells in a unit length, with a mean cell size of μ^{-1}. The above consideration is subject to the restriction that fiber regions cannot overlap, namely $c > h$ ("Gibbs hard core process"). Therefore equation (23) is modified to read

$$P(C > c) = \exp\left(-2\mu'(c-h)\right) \tag{24}$$

Since μ^{-1} is still the expected value of the Voronoi cell size, namely,

$$\mu^{-1} = E(2c) = -\int_h^\infty 2c\frac{d}{dc}P(C > c)\,dc$$

one obtains

$$\mu' = \frac{\mu}{1-2\mu h} \tag{25}$$

Equations (23) - (25) can be expressed in terms of the fiber volume fraction V_f, as employed in equation (13). Let $\overline{V}_f$ denote the average ("nominal") value of the fiber volume fraction and $2\overline{c} = \mu^{-1}$ the average length of the Voronoi cells, then $\overline{V}_f = h/\overline{c} = 2h\mu$. Consequently, we have

$$\mu' = \frac{\overline{V}_f}{2h\left(1-\overline{V}_f\right)}$$

and

$$P(C > c) = \exp\left[-\frac{\overline{V}_f}{1-\overline{V}_f}\left(\frac{c}{h}-1\right)\right]$$

Therefore, the cumulative probability that the fiber volume fraction $\widetilde{V}_f$ exceeds a value V_f is

$$\widehat{P}\left(\widetilde{V}_f > V_f\right) = 1 - P(C > c) = 1 - \exp\left[-\frac{\overline{V}_f}{1-\overline{V}_f}\left(\frac{1}{V_f}-1\right)\right] \tag{26}$$

The probability density distribution which corresponds to equation (26) is

$$\widehat{p}(V_f) = -\frac{d}{dV_f}\widehat{P}\left(\widetilde{V}_f > V_f\right) = \frac{\overline{V}_f}{1-\overline{V}_f}\frac{1}{V_f^2}\exp\left[-\frac{\overline{V}_f}{1-\overline{V}_f}\left(\frac{1}{V_f}-1\right)\right] \tag{27}$$

Computational results for $\widehat{p}(V_f)$ vs. V_f are shown in Figure 5 for three nominal (average) values of $\overline{V}_f$ ($\overline{V}_f$ = 0.3, 0.6, and 0.9).

The Compressive Response with Randomly Spaced Fibers

The probability density $\widehat{p}(V_f)$ given in equation (27) was incorporated into the formulation expressed in equations (11) and (13) and employed to predict the compressive response of Gr/PEEK (APC-2) composite with $\overline{V}_f$ = 0.6 at a temperature of T = 21°C. Based upon the data of Guynn et al. (1992), the nonlinear shear behavior of the PEEK resin was fitted by a Ramberg-Osgood expression

$$\gamma_{xy}^{m} = \frac{\tau_{xy}^{m}}{G_e^{m}} + \left(\frac{\tau_{xy}^{m}}{A}\right)^{1/n} \tag{28}$$

where G_e^m = 1.3 GPa as in the previous section, A = 94.4 MPa and n = 0.12. In addition, we took $\varepsilon = \delta_o/L$ = 1/200 as before and assumed, somewhat arbitrarily, resin failure to occur at $\gamma_{xy}^{m} = \gamma_u$ = 10%. The latter assumption was guided by the observed tensile failure at $\varepsilon_u \sim$ 4%-5% for PEEK at room temperature reported by Johnston et al. (1991). The shear stress-strain response considered in the foregoing representation is shown in Figure 6.

The solution to equation (13), with Y(0) = 0, $\frac{dY}{dX}\left(\frac{1}{2}\right)$ =0, together with (27) and (28) was obtained numerically. Note that equation (28) was supplemented by $\tau_{xy}^{m} = 0$ for $|\gamma_{xy}^{m}| > \gamma_u$. To implement the numerical solution, the field equation (13) was expressed by finite differences as given by Na (1979), and solved iteratively by a quasi-linearization method.

In the above implementation, the probability distribution function of the Voronoi cells, $\widehat{p}(V_f)$, was evaluated at 100 equally spaced, discrete values of V_f varying between V_f = 0 and V_f = 1.0. With the exception of Figures 12 and 13, all computations were performed for $\overline{V}_f$ = 0.6.

Further details of the numerical schemes are given in the Appendix.

Upon attaining convergence to a prescribed degree of accuracy, the computational program gives the values of v^f, Y, Y′ and Y″, as well as the shortening of the column Δ. Results for the non-dimensionalized lateral deflection v^f/L and for the slope Y vs. X are shown in Figures 7 and 8 for three values of non-dimensional compressive loads λ, namely λ = 10, 20 and 26.4. The latter value corresponds to the buckling load, since no equilibrium configuration could be computed for λ>26.4. The variation of γ_{xy}^{m}, the shear strain in the matrix, vs. the distance X at λ=26.4 is shown by the solid line in Figure 9. This variation is contrasted with the variation of γ_{xy}^{m} vs. X for uniformly spaced fibers at the same load level,

as shown by the dashed line, and against the variation of γ_{xy}^m vs. X for uniformly spaced fibers at λ=29.5, which is the maximal load level attained in the uniformly spaced case, as shown by the dotted line. All the plots in Figure 9 correspond to $V_f = 0.6$ (in the case of random spacing $\overline{V}_f = 0.6$ and the results are plotted for the cell with $V_f = 0.6$).

Substitution of the numerically obtained solution for v^f into equation (6) determines the lateral load q(x) for each Voronoi cell, as specified by its fiber volume fraction V_f. Results for q vs. the non-dimensional distance X = x/L are shown in Figure 10 for a typical "matrix rich" cell, with $V_f = 0.25$, at load levels corresponding to λ = 10, 20 and the buckling value λ = 26.4. Similar plots are shown in Figure 11 for a "matrix poor" Voronoi cell, with $V_f = 0.95$. Note that sufficiently low levels of λ, i.e. λ = 10, yield small values of lateral load q, while increasing levels of λ raise the magnitude of q. It is especially interesting to note the "spikes" in the plots of q vs. X. These localized amplifications occur at places where γ_{xy}^m attains its ultimate value γ_u at some Voronoi cell, with the sharpest spike located near the place where $|\gamma_{xy}^m| = \gamma_u$ at the Voronoi cell under consideration. For instance, the spikes in q(X) for λ = 20 in Figure 10 occur at X = 0.15 and X = 0.3, which are the locations where $|\gamma_{xy}^m| = \gamma_u$ at the Voronoi cells of fiber volume fractions $V_f = 0.99$ and $V_f = 0.98$, respectively, at λ = 20. (Obviously, the matrix material in those cells failed over the ranges of $0.15 < X < 0.5$ and $0.3 < X < 0.5$, respectively). On the other hand, the sharp spike at X = 0.25 for λ = 26.4 in Figure 11 is associated with γ_{xy}^m attaining its ultimate value γ_u within the very same Voronoi cell (with $V_f = 0.95$) considered in that figure, while the remaining peaks are associated with shear failures in other cells. Peaks which occur at locations $X < 0.25$ are due to failures in cells with values of $V_f > 0.95$, while spikes located at $X > 0.25$ are due to failures within more resin-rich Voronoi cells.†

Comparison between Figures 10 and 11 shows that resin-rich Voronoi cells are subjected to relatively lower lateral loads. This observation is attributable to the fact that the above mentioned cells sustain shear strains γ_{xy}^m of comparatively smaller magnitudes.

Predicted axial-stress axial-strain relations and compressive strengths under monotonically increasing compressive loads are illustrated in Figure 12 for various values of $\overline{V}_f$. The continuous lines, terminating at points which corresponds to failure, correspond to uniformly spaced fibers, while symbols represent computational results for the case of

†It may seem that lateral equilibrium is not satisfied for the individual Voronoi cells since $\int_0^{1/2} q(X)dX \neq 0$ in the plots shown in Figures 10 and 11. However, due to symmetry about X = 0 and X = 0.5, $\int_0^1 q(X)dX$ indeed vanishes.

randomly spaced Voronoi cells with filled symbols representing failure. The stress-strain responses shown in Figure 12 are dominated by the last term on the right side of equation (4) and thus remain nearly linear until failure. In Figure 13, predicted levels of compressive strength are plotted versus fiber volume fraction, V_f, for uniformly and randomly spaced fibers. Note that random spacings yield lower values of compressive strength and suggest a linear relation between strength and V_f, which accords with experimentally observed trends by Piggott and Harris (1980).

Figures 14 (a, b) exhibit plots of fiber curvatures versus non-dimensional distance X at various levels of non-dimensional compressive load λ. Note the significant increase in curvature for the randomly spaced case (Figure 14 (b)), as compared with the uniformly spaced case (Figure 14 (a)). If, according to Yin (1992), kinks occur when fibers' curvature attains a critical value, then Figures 14 suggest that random spacing yield kinks at lower load levels.

Unlike the circumstance of uniformly spaced fibers with bi-linear shear response of the matrix, the computational scheme for randomly spaced fibers cannot be extended to predict post-buckling behavior such as shown in Figure 2. The specific values of the computed compressive failure stresses are listed in Table 1. That Table exhibits the effects of the nominal volume fraction $\overline{V}_f$, the amplitude of geometric imperfection δ_o/L, and the presence or absence of an ultimate value of matrix shear strain γ_u. The Table also illuminates the effect of random fiber spacing.

3. CONCLUDING REMARKS

This article presented a mechanics model for the compressive response and failure of uni-directionally reinforced polymeric composites loaded parallel to the fiber direction. The model accounted for the non-linear shear response of the resin, including its ultimate shear strain, and incorporated two kinds of geometric imperfections, namely, initial fiber waviness and random fiber spacings. Heretofore, the latter kind of imperfection has not been considered elsewhere.

The non-linear response of the matrix was accounted for by means of the non-linear field equation (6) for the lateral displacement v^f. In general, the above equation could be solved numerically up to failure. Nevertheless, in some special circumstances, it was possible to generate a solution into the post buckling range.

Both kinds of geometric imperfections, initial fiber waviness and random fiber spacings, were shown to substantially reduce the compressive strength of the composite. However, random fiber spacings, when combined with the foregoing non-linear shear response of the matrix, was shown to introduce imbalances in the support furnished by the matrix

against fiber microbuckling — resulting in highly localized internal transverse loads on the fibers. The emergence of these transverse loads alludes to the possibility of transition from microbuckling to microkinking of the deformed fibers. However, it is impossible to explore this matter any further within the context of the Bernoulli-Euler beam theory utilized in the present article since this theory cannot account for discontinuous shear deformations within the fibers. Such discontinuities are likely to occur at locations where the matrix reaches its ultimate strength and ceases to support the fibers, and the highly concentrated transverse loads predicted by the present analysis reflect the indeterminacy inherent in the Bernoulli-Euler theory in addressing shear response.

A remedy to the above inadequacy may be found by emplo[illegible] shear-deformation models, such as the Timoshenko beam theory, to represent the resp[illegible] of the fibers. This approach was employed recently by Chung and Weitsman (1993), where it was shown that random fiber spacing indeed causes discontinuities in the shear strains within the fibers. These discontinuities indicate the emergence of kinks.

ACKNOWLEDGMENT

This work was performed under Contract N00014-90-J-1556 from the Office of Naval Research to one of the authors (YW). The authors wish to thank the program manager, Dr. Y. Rajapakse of the Mechanics Division, Engineering Sciences Directorate, for his encouragement and support.

REFERENCES

Blake, H. W., and Starbuck, J. M. (1993). Hydrostatic Testing of Thick Laminated Composite Cylinders for Performance Model Validation. *Report ORNL/ATD-67*, Oak Ridge National Laboratory, March 1993.

Budiansky, B. and Fleck, N. A. (1992). Compressive Failure of Fibre Composites. *Journal of Mechanics and Physics of Solids*, 41, 193-211.

Camponeschi, Jr., E. T. (1991). Compression of Composite Materials: A Review. *Composite Materials: Fatigue and Fracture, ASTM STP 1110*, 550-578.

Chung, I. and Weitsman, Y. J. (1993). A Model for the Micro-Buckling/Micro-Kinking Compressive Response of Fiber-Reinforced Composites (To appear in Proceedings of the 12th U. S. National Conference of Applied Mechanics, Seattle, WA, 1994).

Davis, Jr., J. G. (1975). Compressive Strength of Fiber-Reinforced Composite Materials. *Composite Reliability, ASTM STP 580*, 364-377.

Davy, P. J. and Guild, F. J. (1988). The Distribution of Interparticle Distance and Its Application in Finite Element Modeling of Composite Materials. *Proceedings of Royal Society*, A418, 95-112.

Evans, A. G. and Adler, W. F. (1978). Kinking as a Mode of Structural Degradation in Cabon Fiber Composites. *Acta Metallurgica*, 26, 725-738.

Garg. S. K., Svalbonas, V., and Gurtman, G. A. (1973). Analysis of Structural Composite Materials, M. Dekker Inc., New York (1973).

Greszczuk, L. B. (1975). Microbuckling Failure of Circular Fiber-Reinforced Composites. *AIAA Journal*, 13, 1311-1318.

Guynn, E. G., Ochoa, O. O., and Bradley, W. L. (1992). A Parametric Study of Variables That Affect Fiber Microbuckling Initiation in Composite Laminates: Part 1 Analyses. *Journal of Composite Materials*, 26, 1594-1616.

Hahn, H. T. and Williams, J. G. (1986). Compression Failure Mechanisms in Unidirectional Composites. *Composite Materials: Testing and Design, ASTM STP 893*, 115-139.

Hermann, L. R., Mason, W. E., and Chan, S. T. K. (1967). Response of Reinforcing Wires to Compressive States of Stress. *Journal of Composite Materials*, 1, 212-226.

Highsmith, A. L., Davis, J. J., and Helms, K. L. E. (1992). The Influence of Fiber Waviness on the Compressive Behavior of Unidirectional Continuous Fiber Composites. *Composite Materials: Testing and Design, ASTM STP 1120*, 20-36.

Johnston, N. J., Towell, T. W., and Hergenrother, P. M. (1991). Physical and Mechanical Properties of High Performance Thermoplastic Polymers and Their Composites. *Thermoplastic Composite Materials* edited by Carlsson, L. A., Elsevier Science Publishers, 27-71.

Lanir, Y. and Fung, Y. C. B. (1972). Fiber Composite Columns under Compression. *Journal of Composite Materials*, 6, 387-401.

Lin, K. Y. and Zhang, X. J. (1992). Effect of Fiber Waviness on the Compressive Strength of Laminated Composites. *Proceedings of the 2nd International Symposium on Composite Materials and Structures*, Beijing, China, 120-125.

Morley, J. G. (1987). High Performance Fiber Composites, Academic Press.

Na, T. Y. (1979). Computational Methods in Engineering Boundary Value Problems, Academic Press.

Piggott, M. R. and Harris, B. (1980). Compression Strength of Carbon, Glass and Kevlar-49 Fibre Reinforced Polyester Resins. *Journal of Materials Science*, 15, 2523-2538.

Piggott, M. R. (1993). Compressive Strength of Composites: How to Measure It and How to Improve It. Advanced Composites '93. *Proceedings of the International*

Conference on Advanced Composite Materials (ICACM) Wollongong, Australia, February 15-19, 1993. (Chandra and Dhingra, Eds.) pp. 51-59 TMS. Publication.

Rosen, B. W. (1965). Mechanics of Composite Strengthening. *Fiber Composite Materials*, American Society for Metals, 37-75.

Sadowsky, M. A., Pu, S. L. and Hussain, M. A. (1967). Buckling of Microfibers. *Journal of Applied Mechanics*, 34, 1011-1016.

Shuart, M. J. (1989). Failure of Compression Loaded Multidirectional Composite Laminates, *AIAA Journal*, 27, 1274-1279.

Shuart, M. J. (1985). Short-Wavelength Buckling and Shear Failures for Compression-Loaded Composite Laminates. *NASA TM*, 87640 (1985).

Simitses, G. J. (1976). An Introduction to the Elastic Stability of Structures, Prentice-Hall, Inc.

Steif, P. S. (1988). A Simple Model for the Comrpessive Failure of Weakly Bonded Fiber Reinforced Composites. *Journal of Composite Materials*, 22, 818-828.

Wang, A. S. D. (1978). A Nonlinear Microbuckling Model Predicting the Compressive Strength of Unidirectional Composites. *ASME Paper 78-WA/Aero-1*, 1-8.

Yin, W. L. (1992). A New Theory of Kink Band Formation. *AIAA-92-2552-CP*, 3028-3035.

$\bar{V}_f$	δ_o / L	Uniform Spacing		Random Spacing	
		$\gamma_u = \infty$	$\gamma_u = 0.1$	$\gamma_u = \infty$	$\gamma_u = 0.1$
0.3	0.0025	1360	1360	1381	1292
	0.0050	1103	1103	1116	1029
	0.0075	941	941	947	867
0.6	0.0025	2023	2023	2144	1746
	0.0050	1541	1541	1583	1234
	0.0075	1253	1253	1281	969
0.9	0.0025	4228	4228	4228	2927
	0.0050	2702	2702	2685	1700
	0.0075	2023	2023	2023	1194

Table 1. Comparison of Failure Strength (MPa)

APPENDIX: THE NUMERICAL SCHEME

The nonlinear second order differential equation (13) can be expressed as

$$Y'' = Q(X,Y) \tag{a1}$$

where the prime denotes derivatives with respect to X, and

$$Q(X,Y) = \int_0^1 \hat{p}(V_f)\, \alpha^2(V_f)\,(1-V_f)\, F\left(\frac{Y}{1-V_f}\right) dV_f - \lambda^2 Y - \lambda^2 Y_o$$

An error quantity at i-th iteration step is defined as

$$\phi^{(i)} = Y''^{(i)} - Q(X,Y^{(i)})$$

Consequently, upon employing a Taylor series expansion, the subsequent error quantity is given by

$$\phi^{(i+1)} = \phi^{(i)} + \left(\frac{\partial\phi}{\partial Y}\right)^{(i)}\left(Y^{(i+1)} - Y^{(i)}\right) + \left(\frac{\partial\phi}{\partial Y''}\right)^{(i)}\left(Y''^{(i+1)} - Y''^{(i)}\right) \tag{a2}$$

Noting that $\left(\frac{\partial\phi}{\partial Y}\right)^{(i)} = -\left(\frac{\partial Q}{\partial Y}\right)^{(i)}$ and $\left(\frac{\partial\phi}{\partial Y''}\right)^{(i)} = 1$, we obtain, upon imposing $\phi^{(i)} = \phi^{(i+1)} = 0$ in equation (a2)

$$Y''^{(i+1)} - \left(\frac{\partial Q}{\partial Y}\right)^{(i)} Y^{(i+1)} = Q(X,Y^{(i)}) - \left(\frac{\partial Q}{\partial Y}\right)^{(i)} Y^{(i)} \tag{a3}$$

Expression (a3) is a linear ordinary differential equation for $Y^{(i+1)}$ involving the known results of the previous iteration $Y^{(i)}$. Note that the derivative of Q with respect to Y is

$$\frac{\partial Q}{\partial Y} = \int_0^1 \hat{p}(V_f)\, \alpha^2(V_f)\;\; F'\left(\frac{Y}{1-V_f}\right) dV_f - \lambda^2$$

Furthermore, upon employment of the Ramberg-Osgood model, we have

$$F' = \frac{1}{1 + \frac{G_e^m}{A^{1/n}n}\left(\tau_{xy}^m\right)^{\frac{(1-n)}{n}}}$$

Obviously, the boundary conditions in equation (15) must be satisfied in every iteration step.

The linear differential equation (a3) is solved by a finite difference scheme as follows. Divide the abscissa 0<X<1 into N equal intervals of length h=1/N. Then at each node $X=X_n=nh$ the second derivative Y" is expressed as

$$Y''_n = \frac{1}{h^2}\left(Y_{n+1} - 2Y_n + Y_{n-1}\right)$$

Using the above relation, equation (a3) can be converted to an algebraic equation of the form

$$Y_{n-1}^{(i+1)} + b_n^{(i+1)} Y_n^{(i+1)} + Y_{n+1}^{(i+1)} = r_n^{(i+1)} \tag{a4}$$

Here,

$$b_n^{(i+1)} = -h^2 \left(\frac{\partial Q}{\partial Y}\right)_n^{(i)} - 2$$

$$r_n^{(i+1)} = h^2 \left\{ Q(X_n, Y_n^{(i)}) - \left(\frac{\partial Q}{\partial Y}\right)_n^{(i)} Y_n^{(i)} \right\}$$

The boundary conditions in finite difference scheme are $Y_0^{(i+1)} = 0$ and $Y_{N+1}^{(i+1)} = Y_{N-1}^{(i+1)}$.

The system of equations (a4) can be represented as

$$A^{(i+1)} Y^{(i+1)} = S^{(i+1)} \tag{a5}$$

where

$$A^{(i+1)} = \begin{bmatrix} b_1^{(i+1)} & 1 & & & & 0 \\ 1 & b_2^{(i+1)} & 1 & & & \\ & 1 & b_3^{(i+1)} & 1 & & \\ & & & \ddots & & \\ & & & 1 & b_{N-1}^{(i+1)} & 1 \\ 0 & & & & 2 & b_N^{(i+1)} \end{bmatrix} \quad Y^{(i+1)} = \begin{pmatrix} Y_1^{(i+1)} \\ Y_2^{(i+1)} \\ \vdots \\ Y_N^{(i+1)} \end{pmatrix} \quad S^{(i+1)} = \begin{pmatrix} r_1^{(i+1)} \\ r_2^{(i+1)} \\ \vdots \\ r_N^{(i+1)} \end{pmatrix}$$

Equation (a5) can be solved by means of the LU decomposition (Na, 1979). Accordingly, the matrix $A^{(i+1)}$ is decomposed into the product $A^{(i+1)} = L^{(i+1)} U^{(i+1)}$.

Here,

$$L^{(i+1)} = \begin{bmatrix} \beta_1^{(i+1)} & & & & 0 \\ 1 & \beta_2^{(i+1)} & & & \\ & & \ddots & & \\ & & 1 & \beta_{N-1}^{(i+1)} & \\ 0 & & & 2 & \beta_N^{(i+1)} \end{bmatrix} \quad U^{(i+1)} = \begin{bmatrix} 1 & \gamma_1^{(i+1)} & & & 0 \\ & 1 & \gamma_2^{(i+1)} & & \\ & & \ddots & & \\ & & & 1 & \gamma_{N-1}^{(i+1)} \\ 0 & & & & 1 \end{bmatrix}$$

and

$$\beta_1^{(i+1)} = b_1^{(i+1)}$$
$$\beta_n^{(i+1)}\gamma_n^{(i+1)} = 1 \quad (n = 1,2... N-1)$$
$$\beta_n^{(i+1)} = b_n^{(i+1)} - \gamma_{n-1}^{(i+1)} \quad (n = 2,3...N-1)$$
$$\beta_N^{(i+1)} = b_N^{(i+1)} - 2\gamma_{N-1}^{(i+1)}$$

Denoting

$$Z^{(i+1)} = U^{(i+1)} Y^{(i+1)} \tag{a6}$$

equation (a5) is transformed to $L^{(i+1)}Z^{(i+1)} = S^{(i+1)}$, where the components of $Z^{(i+1)}$ are computed by

$$z_1^{(i+1)} = r_1^{(i+1)} / \beta_1^{(i+1)}$$
$$z_n^{(i+1)} = \left(r_n^{(i+1)} - z_{n-1}^{(i+1)}\right) / \beta_n^{(i+1)} \quad (n = 2,3...N-1)$$
$$z_N^{(i+1)} = \left(r_N^{(i+1)} - 2z_{N-1}^{(i+1)}\right) / \beta_N^{(i+1)}$$

The recursive relations between $z_n^{(i+1)}$'s and $Y_n^{(i+1)}$'s are obtained from equation (a6) as

$$Y_N^{(i+1)} = z_N^{(i+1)}$$
$$Y_n^{(i+1)} = z_n^{(i+1)} - \gamma_n^{(i+1)} Y_{n+1}^{(i+1)} \quad (n= N-1,N-2,...,1)$$

The values of $Y_n^{(i+1)}$ express the solution to equation (13) at the (i+1)th iterative step. When $\sum_{n=1}^{N} \left|Y_n^{(i+1)} - Y_n^{(i)}\right|^2$ attains a constant value within a prescribed tolerance, the iteration is halted and post-processed to compute deflection, shear strain and stress, lateral stress and other quantities.

<u>List of Figures</u>

Figure 1. (a) A fiber composite modelled as a two dimensional lamellar region consisting of fiber and matrix plates; (b) a deformed single cell.

Figure 2. The scaled compressive displacement Δ/L at $X=0.5$ vs. applied compressive stress σ_c for various fiber volume fractions V_f (symbol "+" corresponds to the circumstance of $\left|\gamma^m_{xy}(X=\frac{1}{2})\right| = \gamma_y$).

Figure 3. The dimensionless length, $\hat{\xi} = 0.5 - \xi$, of the inelastic zone of matrix shear response ($|\gamma^m_{xy}| > \gamma_y$ in equation (18)) vs. applied compressive stress for V_f = 0.3, 0.6 and 0.9.

Figure 4. The variation of the matrix shear strain γ^m_{xy} vs. the non-dimensionalized distance X along the fiber/matrix interface at several values of non-dimensionalized applied compressive stress λ. Fiber volume fraction V_f = 0.6. Onset of departure from linear elastic matrix shear response at $\lambda = \lambda_y$ = 30.79, maximum compressive stress at $\lambda = \lambda_{max}$ = 30.81.

Figure 5. Distribution of local fiber volume fraction for randomly spaced fiber composites with average fiber volume fraction, $\overline{V}_f$, of 0.3, 0.6 and 0.9.

Figure 6. Shear constitutive relation of PEEK at 21°C based on Guynn's (1992) estimation with shear failure strain assumed at 10%.

Figure 7. Non-dimensionalized deflection, v^f/L, vs. X for randomly spaced fiber composite with $\overline{V}_f$ = 0.6, under compressive loads corresponding to λ = 10, 20 and 26.4. Failure shear strain γ_u is 10%, and λ = 26.4 is the compressive strength of the composite.

Figure 8. Solution Y of the governing equation for randomly spaced fiber composite with $\overline{V}_f$ = 0.6, under compressive loads corresponding to λ = 10, 20 and 26.4. Failure shear strain γ_u is 10%, and λ = 26.4 is the compressive strength of the composite.

Figure 9. Comparison between the matrix shear strain within the Voronoi cell with V_f = 0.6 in randomly spaced fiber composite under its failure load λ = 26.4 and the matrix shear strain for uniformly spaced fiber composite under the same load level as well as with its own failure load λ = 29.5. $\overline{V}_f$ is 0.6 for both cases (RS and US designate randomly and uniformly spaced fiber composite, respectively).

Figure 10. Lateral stress q(X) vs. X on a Voronoi cell with $V_f = 0.25$ in randomly spaced fiber composite with $\overline{V}_f = 0.6$ at various levels of non-dimensional compressive loads λ. The load $\lambda = 26.4$ corresponds to the failure strength of the composite.

Figure 11. Lateral stress q(X) vs. X on a Voronoi cell with $V_f = 0.95$ in randomly spaced fiber composite with $\overline{V}_f = 0.6$ at various levels of non-dimensional compressive loads λ. The load $\lambda = 26.4$ corresponds to the failure strength of the composite.

Figure 12. Dimensionless displacement $-\Delta/L$ at X=0.5 vs. applied compressive stress. (Solid lines are for uniformly spaced fiber composite. Symbols are for randomly spaced fiber composite. The ends of lines and the filled symbols indicate compressive failure strength for uniform and random spacings, respectively.)

Figure 13. Compressive strengths of uniformly and randomly spaced fiber composites vs. fiber volume fraction.

Figure 14. Pre-buckling Curvature of fiber layer in the case of (a) Uniformly spaced fiber composite and (b) Randomly spaced fiber composite. In both cases $\overline{V}_f = 0.6$.

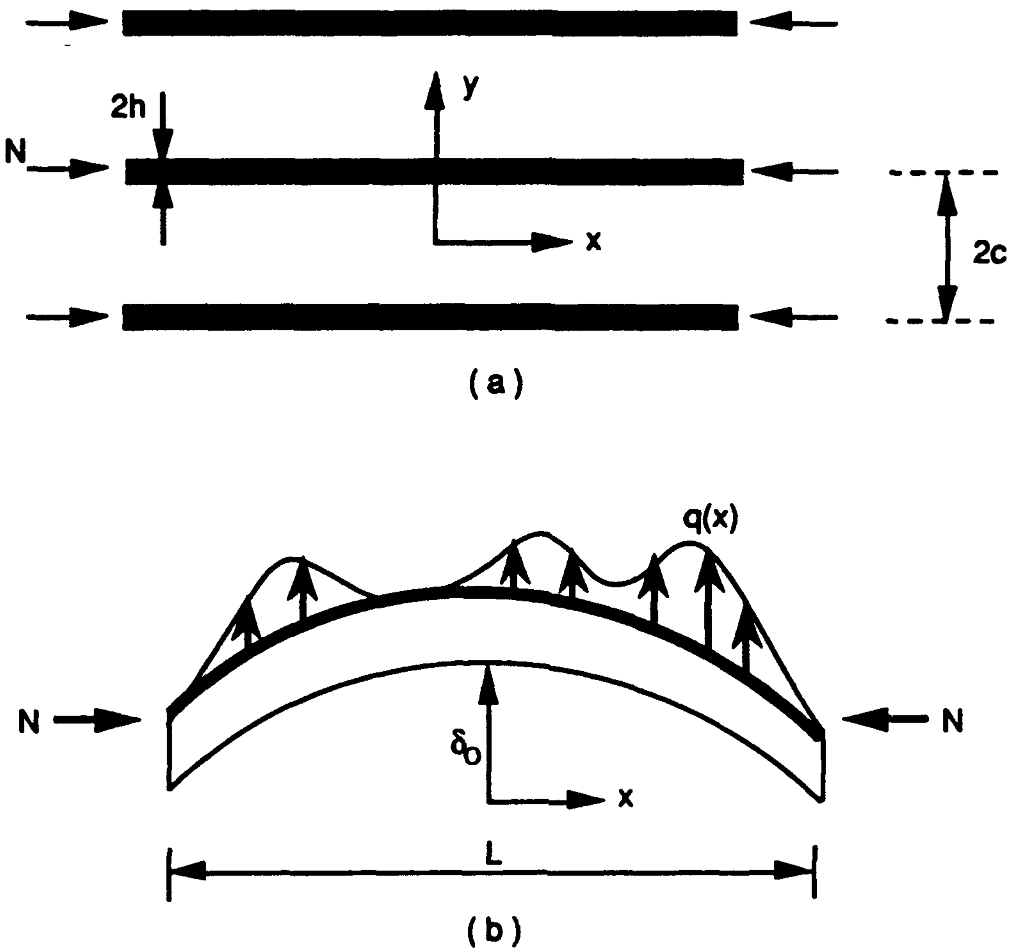

Figure 1. (a) A fiber reinforced composite modelled as a two dimensional lamellar region consisting of fiber and matrix plates; (b) a deformed single cell.

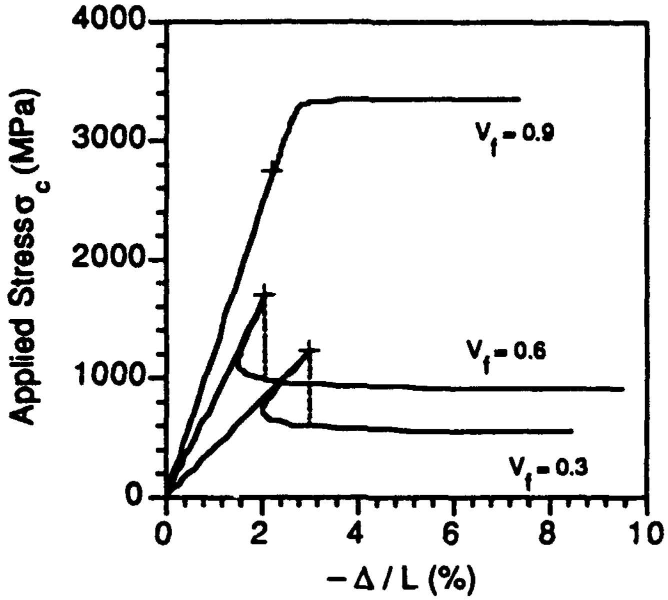

Figure 2. The scaled compressive displacement Δ/L at $X=0.5$ vs. applied compressive stress σ_c for various fiber volume fractions V_f (symbol "+" corresponds to the circumstance of $\left|\gamma^m_{xy}(X=\frac{1}{2})\right| = \gamma_y$).

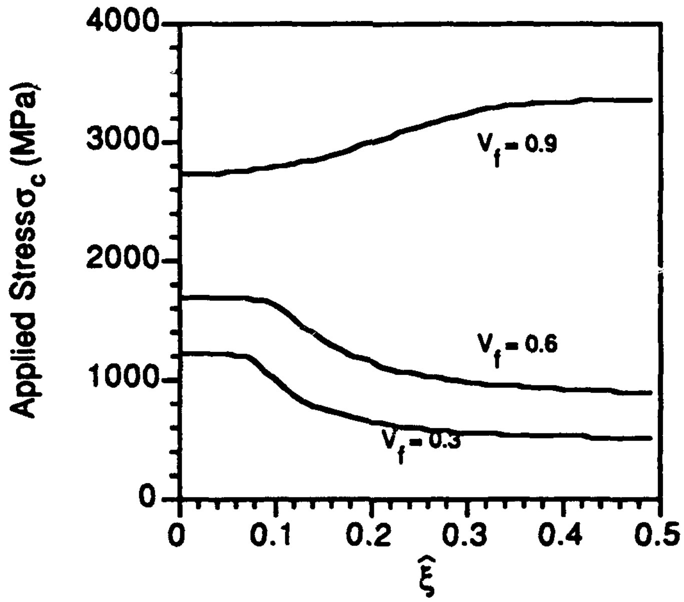

Figure 3. The dimensionless length, $\hat{\xi} = 0.5 - \xi$, of the inelastic zone of matrix shear response ($|\gamma^m_{xy}| > \gamma_y$ in equation (18)) vs. applied compressive stress for $V_f = 0.3$, 0.6 and 0.9.

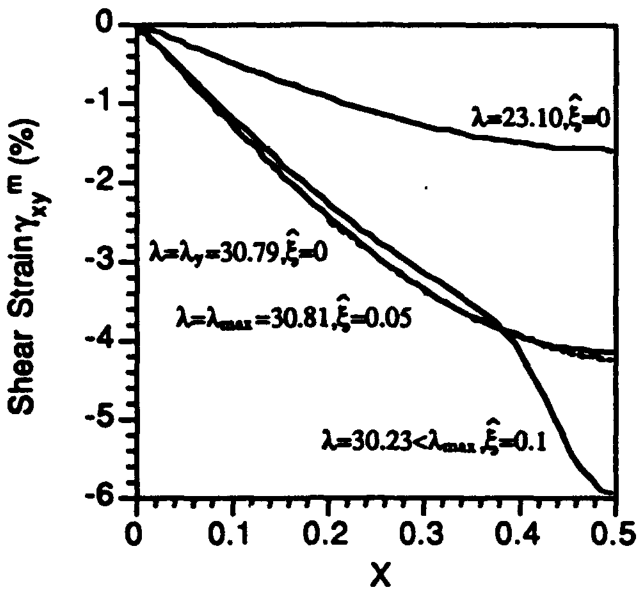

Figure 4. The variation of the matrix shear strain γ_{xy}^m vs. the non-dimensionalized distance X along the fiber/matrix interface at several values of non-dimensionalized applied compressive stress λ. Fiber volume fraction $V_f = 0.6$. Onset of departure from linear elastic matrix shear response at $\lambda = \lambda_y = 30.79$, maximum compressive stress at $\lambda = \lambda_{max} = 30.81$.

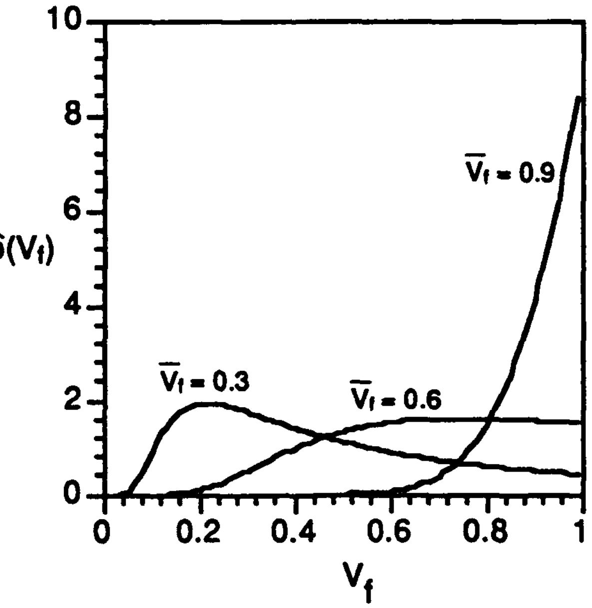

Figure 5. Distribution of local fiber volume fraction for randomly spaced fiber composites with average fiber volume fraction, $\overline{V}_f$, of 0.3, 0.6 and 0.9.

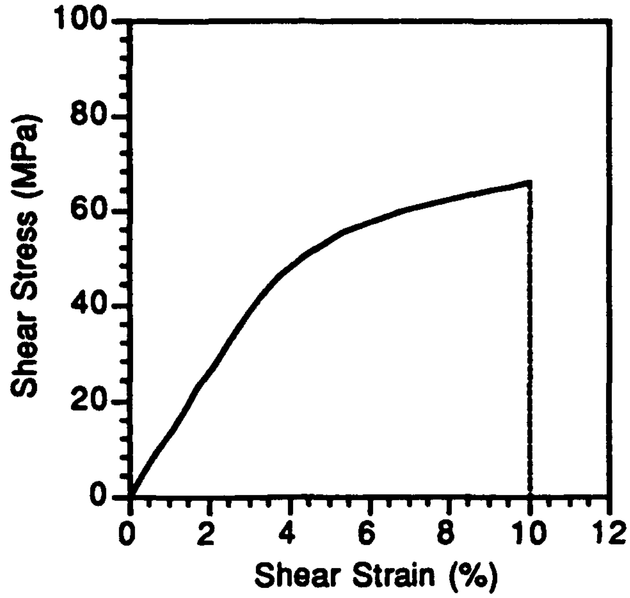

Figure 6. Shear constitutive relation of PEEK at 21°C based on Guynn's (1992) estimation with shear failure strain assumed at 10%.

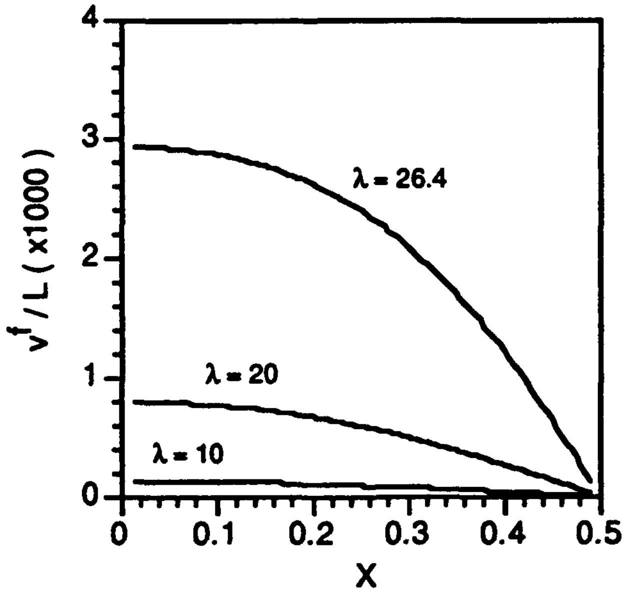

Figure 7. Non-dimensionalized deflection, v^f/L, vs. X for randomly spaced fiber composite with $\overline{V}_f = 0.6$, under compressive loads corresponding to $\lambda = 10$, 20 and 26.4. Failure shear strain γ_u is 10%, and $\lambda = 26.4$ is the compressive strength of the composite.

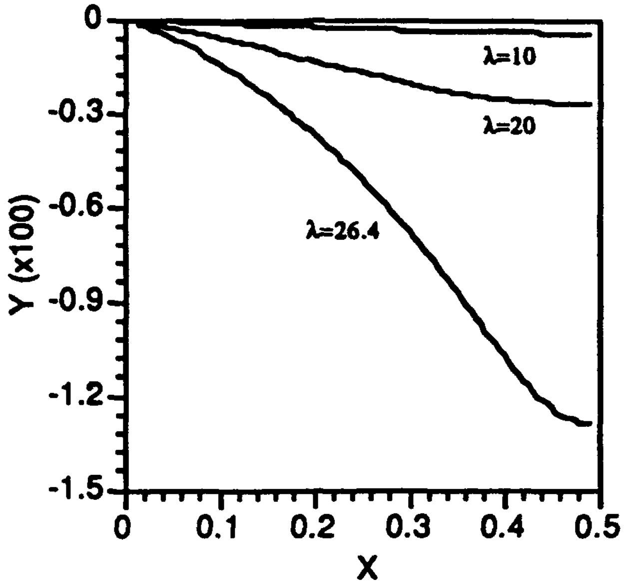

Figure 8. Solution Y of the governing equation for randomly spaced fiber composite with $\overline{V}_f = 0.6$, under compressive loads corresponding to $\lambda = 10$, 20 and 26.4. Failure shear strain γ_u is 10%, and $\lambda = 26.4$ is the compressive strength of the composite.

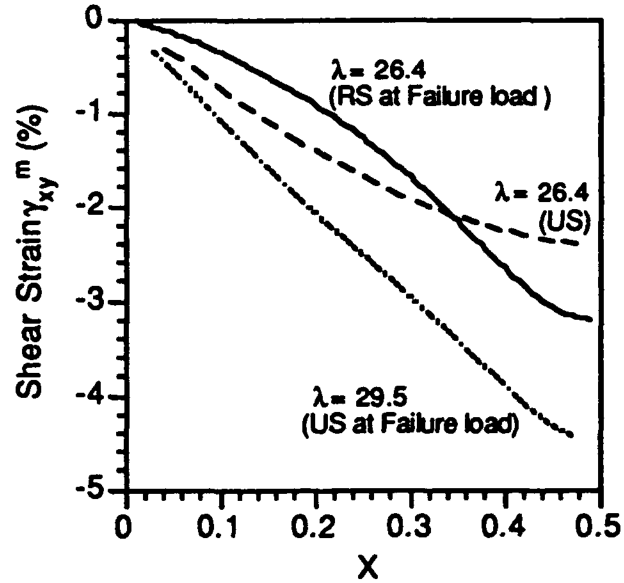

Figure 9. Comparison between the matrix shear strain of the Voronoi cell with $V_f = 0.6$ in randomly spaced fiber composite under its failure load $\lambda = 26.4$ and the matrix shear strain for uniformly spaced fiber composite under the same load level as well as with its own failure load $\lambda = 29.5$. $\overline{V}_f$ is 0.6 for both cases (RS and US designate randomly and uniformly spaced fiber composite, respectively).

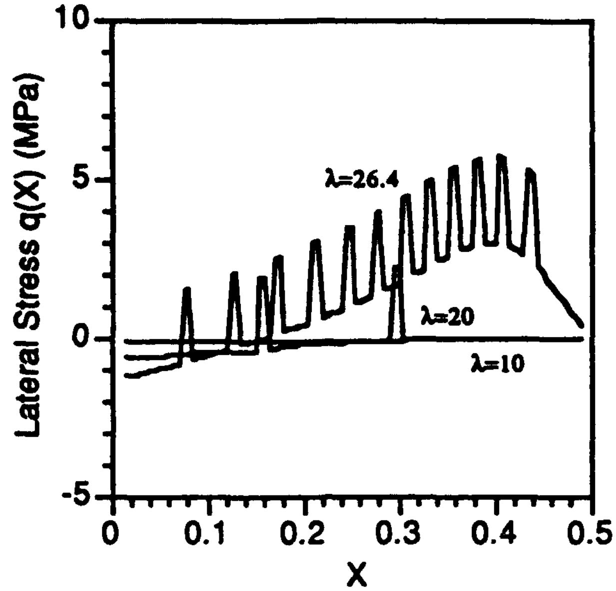

Figure 10. Lateral stress q(X) vs. X on a Voronoi cell with $V_f = 0.25$ in randomly spaced fiber composite with $\overline{V}_f = 0.6$ at various levels of non-dimensional compressive loads λ. The load $\lambda = 26.4$ corresponds to the failure strength of the composite.

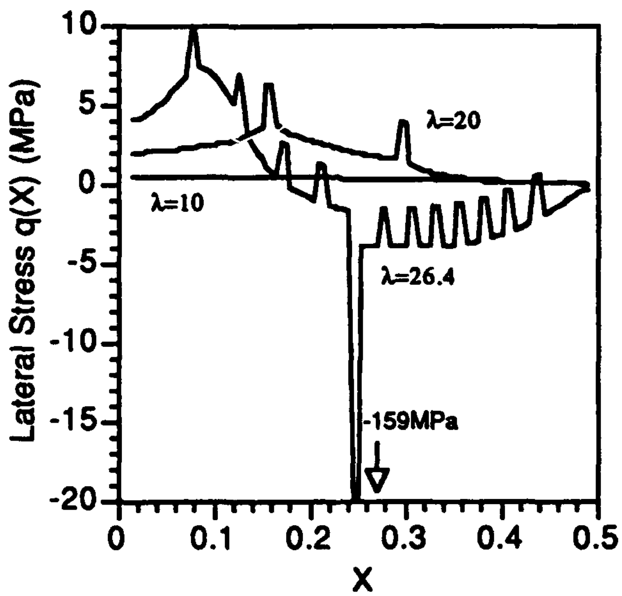

Figure 11. Lateral stress q(X) vs. X on a Voronoi cell with $V_f = 0.95$ in randomly spaced fiber composite with $\overline{V}_f = 0.6$ at various levels of non-dimensional compressive loads λ. The load $\lambda = 26.4$ corresponds to the failure strength of the composite.

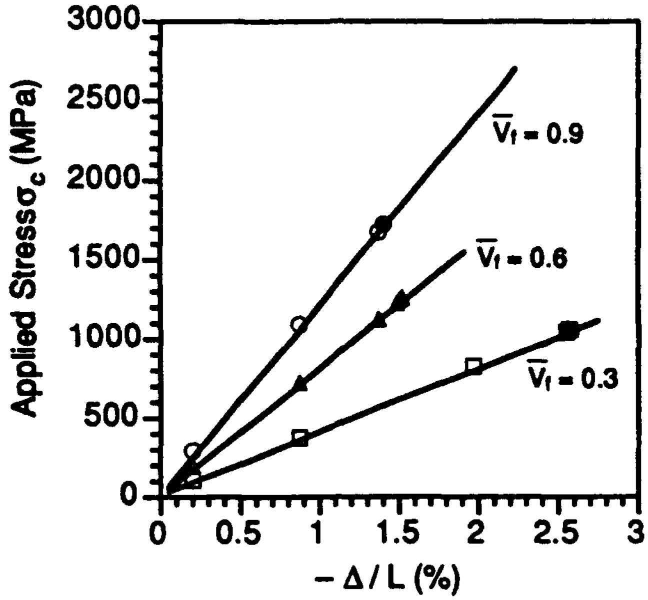

Figure 12. Dimensionless displacement $-\Delta/L$ at X=0.5 vs. applied compressive stress. (Solid lines are for uniformly spaced fiber composite. Symbols are for randomly spaced fiber composite. The ends of lines and the filled symbols indicate compressive failure strength for uniform and random spacings, respectively.)

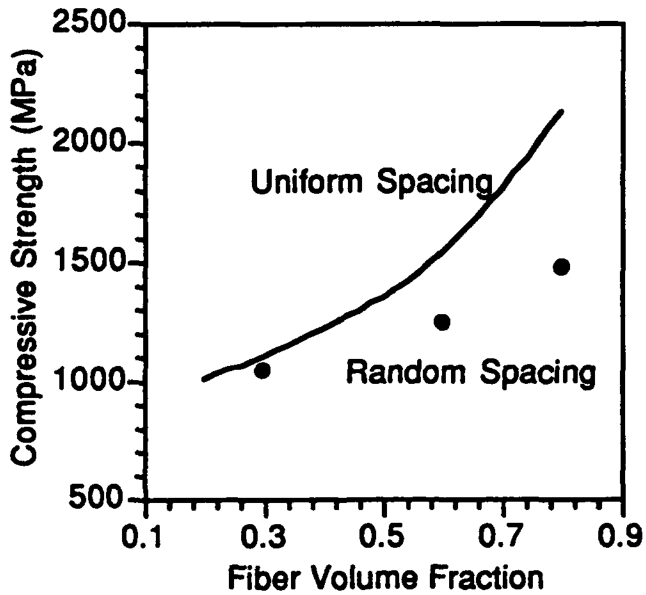

Figure 13. Compressive strengths of uniformly and randomly spaced fiber composites vs. fiber volume fraction.

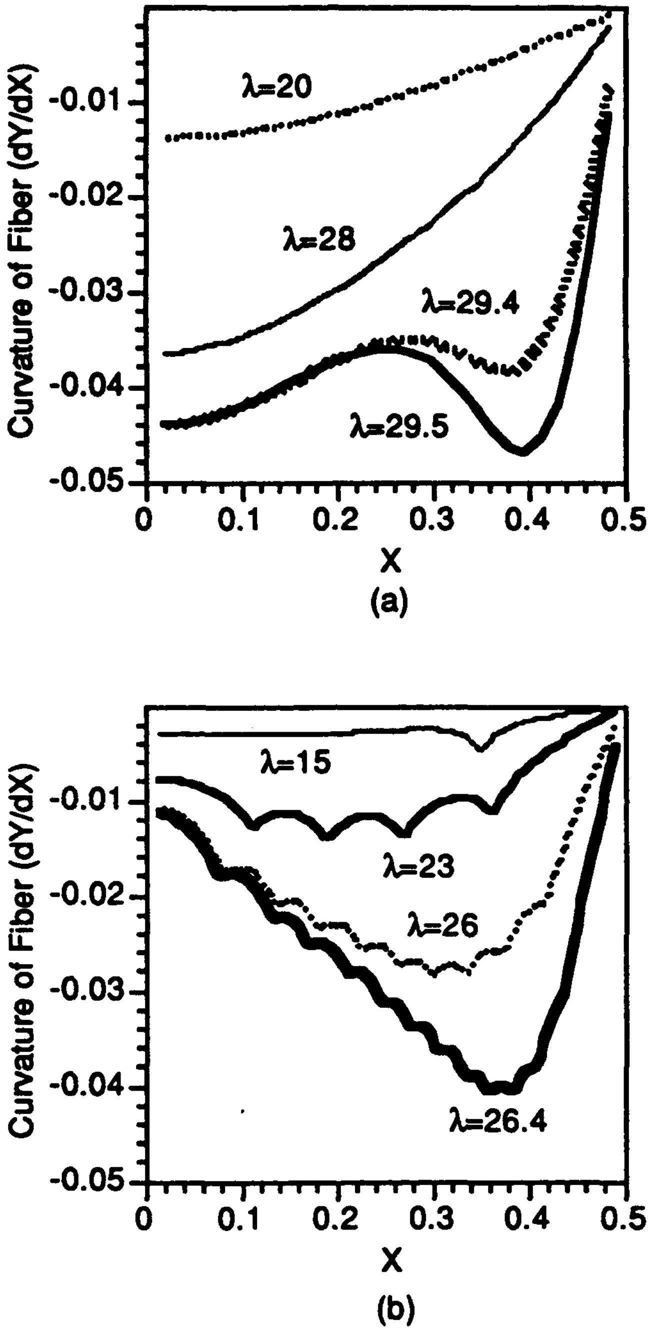

Figure 14. Pre-buckling Curvature of fiber layer in the case of (a) Uniformly spaced fiber composite and (b) Randomly spaced fiber composite. In both cases $\overline{V}_f = 0.6$.